On the Presence of a Universal Acceleration Scale in Elliptical Galaxies

Kyu-Hyun Chae[1] , Mariangela Bernardi[2], Helena Domínguez Sánchez[2,3], and Ravi K. Sheth[2]

[1] Department of Physics and Astronomy, Sejong University, 209 Neungdong-ro Gwangjin-gu, Seoul 05006, Republic of Korea; chae@sejong.ac.kr, kyuhyunchae@gmail.com

[2] Department of Physics and Astronomy, University of Pennsylvania, 209 South 33rd Street, Philadelphia, PA 19104, USA

[3] Institute of Space Sciences (ICE, CSIC), Campus UAB, Carrer de Magrans, E-08193 Barcelona, Spain

Abstract

Dark matter phenomena in rotationally supported galaxies exhibit a characteristic acceleration scale of $g_\dagger \approx 1.2 \times 10^{-10}$ m s^{-2}. Whether this acceleration is a manifestation of a universal scale, or merely an emergent property with an intrinsic scatter, has been debated in the literature. Here we investigate whether a universal acceleration scale exists in dispersion-supported galaxies using two uniform sets of integral field spectroscopy (IFS) data from SDSS-IV MaNGA and ATLAS^{3D}. We apply the spherical Jeans equation to 15 MaNGA and 4 ATLAS^{3D} slow-rotator E0 (i.e., nearly spherical) galaxies. Velocity dispersion profiles for these galaxies are well determined with observational errors under control. Bayesian inference indicates that all 19 galaxies are consistent with a universal acceleration of $g_\dagger = 1.5^{+0.9}_{-0.6} \times 10^{-10}$ m s^{-2}. Moreover, all 387 data points from the radial bins of the velocity dispersion profiles are consistent with a universal relation between the radial acceleration traced by dynamics and that predicted by the observed distribution of baryons. This universality remains if we include 12 additional non-E0 slow-rotator elliptical galaxies from ATLAS^{3D}. Finally, the universal acceleration from MaNGA and ATLAS^{3D} is consistent with that for rotationally supported galaxies, so our results support the view that dark matter phenomenology in galaxies involves a universal acceleration scale.

1. Introduction

Historically, empirical laws such as Kepler's kinematic laws have played crucial roles in physics. For the study of galaxies, these include the Faber–Jackson (Faber & Jackson 1976) and Fundamental Plane (Djorgovski & Davis 1987; Dressler et al. 1987) relations for pressure-supported early-type galaxies, and the Tully–Fischer (Tully & Fisher 1977), baryonic Tully–Fisher (McGaugh et al. 2000), central density (Lelli et al. 2016), and radial acceleration relations (RARs; McGaugh et al. 2016) for rotationally supported late-type galaxies.

The RAR—a relation between the observed radial (centripetal) acceleration g_{obs} and the expected Newtonian acceleration g_{bar} due to the observed distribution of baryonic matter, for rotationally supported galaxies—is of particular interest as it exhibits a characteristic acceleration scale (denoted $g_\dagger$) for dark matter phenomenology. If this scale is truly universal among all galaxies, it would naturally correspond to the critical acceleration (denoted a_0) of the Modified Newtonian dynamics (MOND) paradigm (Milgrom 1983). On the other hand, if there is an intrinsic galaxy-to-galaxy scatter in $g_\dagger$, MOND would be called into question and $g_\dagger$ must be an emergent property of the dark matter phenomenology and/or the physics of galaxy formation.

When McGaugh et al. (2016) reported the RAR from 153 galaxies selected from the SPARC database (Lelli et al. 2016), they noted that data points from individual galaxies scattered around a universal RAR of $g_\dagger \approx 1.2 \times 10^{-10}$ m s^{-2} with a typical scatter of ~0.1 dex consistent with typical observational errors. Li et al. (2018) carried out Bayesian modeling of individual SPARC galaxies and noted that allowing a broad range of $g_\dagger$ did not improve overall fit qualities compared with the case of fixing (or imposing a narrow range of) $g_\dagger$. Therefore, up to realistic uncertainties, rotation curves of all

rotationally supported galaxies appeared to be consistent with a universal $g_\dagger$.

This view was challenged by several authors (Rodrigues et al. 2018a, 2018b; Chang & Zhou 2019; Marra et al. 2020), who carried out Bayesian modeling using the formal uncertainties of individual rotation curves (and using uninformative priors in some cases). However, Kroupa et al. (2018) and McGaugh et al. (2018) have highlighted the uncertain nature of some formal errors and the issue of appropriate priors, and Cameron et al. (2020) further pointed out the issue of the potential model misspecification in Bayesian applications to galaxy rotation curves arising from problems in data and/or the model.

Stone & Courteau (2019) considered an order-of-magnitude larger collection of rotation curves including the SPARC galaxies as a subsample (the "PROBES" sample) and argued for an intrinsic scatter in the RAR. However, individual rotation curves of the PROBES sample are typically not as accurate and extended as those of SPARC galaxies because they largely come from one-dimensional long-slit Hα spectroscopy, which does not allow for accurate estimates of kinematic inclinations or identification of warped disks and noncircular motions. In addition, Stone & Courteau (2019) considered stellar mass rather than total baryonic mass distributions. However, unlike the SPARC mass models based on homogeneous Spitzer photometry at 3.6 μm, in which the stellar mass-to-light ratio ($M_\star/L$) is approximately constant (e.g., Schombert et al. 2019), the mass models of Stone & Courteau (2019) are based on heterogeneous photometry in different bands, in which variations in $M_\star/L$ are a major concern (e.g. McGaugh & Schombert 2014). Therefore, it is more challenging to test the intrinsic scatter of $g_\dagger$ with PROBES galaxies.

To broaden the discussion of the universality or not of $g_\dagger$, here we consider fitting the RAR to individual *dispersion-supported* elliptical galaxies, which we select from uniform integral field spectroscopic (IFS) surveys: SDSS-IV MaNGA and ATLAS^{3D}. This is attractive for a number of reasons. First, both kinematic and photometric data come from uniform observations while SPARC and PROBES are collections of heterogeneously derived rotation curves. This means that measurement uncertainties of stellar velocity dispersions and light distributions of our galaxies are better understood. Second, we select only nearly spherical, slow-rotator (SR) galaxies and model them with the spherical Jeans equation. Although this means we are left with relatively few objects, modeling complications and errors can be minimized because of the relative simplicity of spherical models. Third, the velocity dispersion profiles of our galaxies cover acceleration ranges that are slightly larger than $g_\dagger$. Although this weakens the sensitivity to $g_\dagger$, it also makes the external field effect less of a concern (see Figure 1 of Chae et al. 2020). Finally, our constraints on $g_\dagger$ are independent of those from rotationally supported galaxies. Thus, our constraints on the universality of $g_\dagger$ in elliptical galaxies can be directly compared with those from rotationally supported galaxies.

As our goal is to test whether a common acceleration scale is present in elliptical galaxies, we will carry out kinematic modeling in the framework of MOND. In Section 2 we describe our methodology and data. We present our results in Section 3, and discuss and conclude in Section 4.

2. Data and Methodology

2.1. Galaxy Samples

As we will use the spherical model, we select galaxies that are morphologically round E0s (defined here to be $b/a > 0.9$ where a and b are the semimajor and semiminor axes of the light distribution) and kinematically SRs. Because reliable kinematic modeling requires accurate velocity dispersion distributions of good spatial resolution, we consider the MaNGA (Bundy et al. 2015) and ATLAS^{3D} (Cappellari et al. 2011) databases. The ATLAS^{3D} database provides velocity dispersion distributions with good spatial resolution but the sample size is small (260); the MaNGA database (not complete at the time of this writing) will eventually provide ~10,000 galaxies but with poorer spatial resolution than ATLAS^{3D} (Bundy et al. 2015) because the objects are more distant.

Of the subsample of 24 disk-less (i.e., pure-bulge) ATLAS^{3D} galaxies selected in Chae et al. (2018, 2019a), 4 are round SRs: NGC 4486, 4636, 5846, and 6703. Their velocity dispersion maps and light distributions are shown in Chae et al. (2018) and references therein.

We select galaxies from the MaNGA DR15 catalog (Aguado et al. 2019) as follows. Based on the photometric and morphological properties presented by Fischer et al. (2019), we require (1) TType <0 (select early-types), (2) $P_{S0} < 0.3$ (small probability of being S0 rather than elliptical), (3) B/T > 0.7 (bulge dominates light), (4) $\varepsilon (\equiv 1 - b/a) < 0.1$ (image is round), (5) $n_{Ser} > 3$ (light is centrally concentrated), and (6) $\lambda_e < 0.08 + \varepsilon/4$ (ensure SRs; see Fischer et al. 2019). Of 4672 MaNGA DR15 galaxies only 30 satisfy these stringent criteria.

The velocity profiles of these galaxies are computed from the kinematic measurements derived by the MaNGA Data Analysis
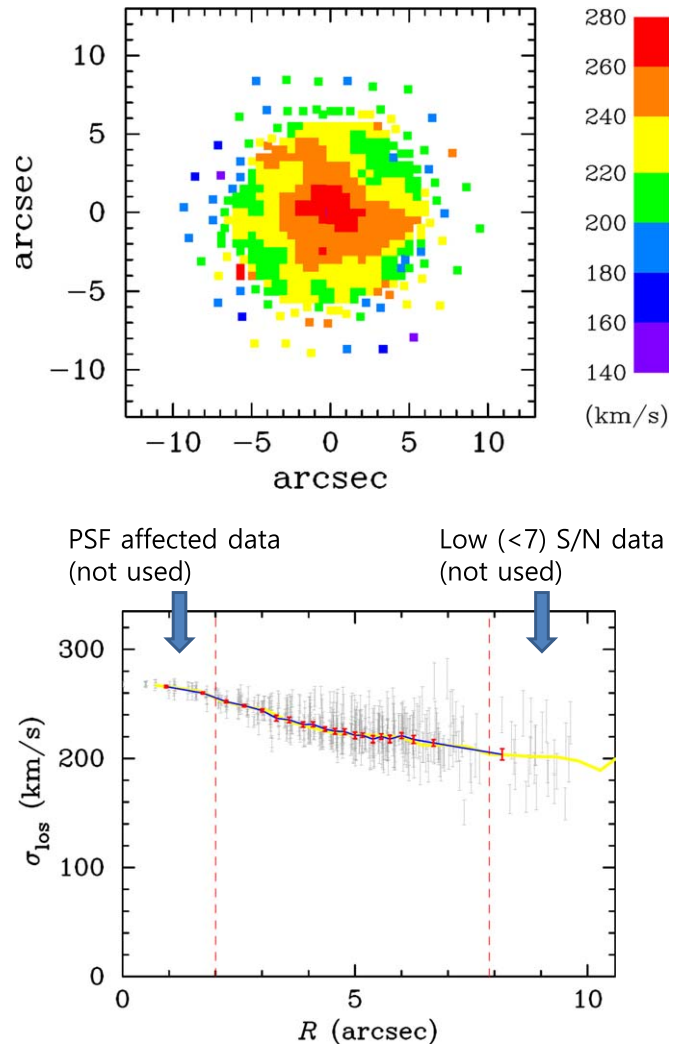

Figure 1. Velocity dispersion map and the constructed radial profile of MaNGA IFU plate 9047-6102. (Top) Line-of-sight velocity dispersions measured at spaxels are represented by different colors. (Bottom) Radial bins are defined by concentric rings, and each bin except for the outermost one contains the same number of spaxels ($N = 25$ in this case). The velocity dispersion in each ring is defined by the mean of the individual values and its uncertainty is defined by the standard deviation of the mean given by rms/$\sqrt{N-1}$. The inner $R < 2''$ region is affected by the finite point-spread function (PSF) size (a diameter of $2''$), and so is not used. Also, low-S/N data in the outer region are not used as indicated.

Pipeline contained in the MAPS-VOR10-GAU-MILESHC. An example is shown in Figure 1. The velocity profile is constructed in two ways. The first one (the yellow line) is the median value of the velocity dispersion of the unmasked spaxels with signal-to-noise ratio (S/N) > 5 in circularized radial bins of equal width. A 3σ clipping is also applied to prevent outliers from affecting the profile shape. The second one (the blue line and red points) is constructed by defining radial bins with an equal number of velocity dispersions ($N \geqslant 11$). Both agree and we use the red points with error bars for our modeling.

A MaNGA velocity dispersion map is discarded if it has too few independent values from which to construct a velocity dispersion radial profile with reasonable estimates of statistical uncertainties, or it is obviously asymmetric and therefore inconsistent with the spherical symmetry assumption, or the constructed radial profile does not cover at least twice the

Table 1
List of MaNGA Selected Slow-rotator E0 Galaxies

IFU Plate	M_r (mag)[a]	a (kpc)[b]	n_{Ser}	b/a
8243-6101	−23.12	21.92	6.411	0.932
8249-6103	−22.50	9.43	5.288	0.946
8323-9101	−22.13	14.69	7.369	0.927
8459-6104	−22.47	10.99	7.245	0.901
8482-1901	−23.05	25.36	8.000	0.908
8555-6101	−23.26	11.98	4.873	0.953
8718-3704	−23.29	17.98	8.000	0.902
8726-9102	−22.96	19.10	8.000	0.928
9024-3701	−21.17	4.74	6.003	0.978
9047-6102	−22.53	13.91	6.965	0.914
9088-3701	−22.26	8.26	8.000	0.923
9485-6102	−23.32	13.29	5.498	0.928
9501-6104	−23.08	16.20	5.080	0.947
9868-3704	−22.25	6.79	5.997	0.906
9888-6102	−23.13	10.18	4.000	0.930

Notes.
[a] SDSS r-band absolute magnitude is from a Sérsic profile truncated at $8R_e$.
[b] Major axis of the ellipse enclosing one-half of the total light of the Sérsic profile assuming $H_0 = 70$ km s^{-1} Mpc^{-1}, $\Omega_{M0} = 0.3$, and $\Omega_{\Lambda0} = 0.7$. The circularized effective radius used for modeling is $R_e \equiv \sqrt{ab}$.

radius affected by the finite fiber size ($2''$). Half of the selected MaNGA galaxies are discarded in this way, and thus we are left with 15 good-quality MaNGA spherical, SR galaxies. This cut based on IFU data quality will, of course, not be biased against any particular value of $g_†$.

The selected 15 MaNGA SR E0s are listed in Table 1. These are all *luminous giant ellipticals* brighter than a characteristic luminosity L_* and larger than ≈ 5 kpc.

2.2. Methodology

The observed two-dimensional map of line-of-sight velocity dispersions that defines a radial profile $\sigma_{\mathrm{los}}(R)$ provides all the dynamical constraints for our models. Figure 1 shows an example of good-quality MaNGA velocity dispersions and the range of scales that is actually used for kinematic modeling.

In our modeling we allow for velocity dispersion anisotropies and stellar mass-to-light ratio ($M_\star/L$) radial gradients. We follow the modeling procedures used recently (Chae et al. 2018, 2019b). All our galaxies have negligible amounts of cold gas in the IFU-probed regions, so throughout baryons mean stars. Here we describe briefly the essential elements.

We work in the MOND framework in which the empirical[4] (i.e., dynamical) radial acceleration $g_{\mathrm{dyn}}(r)$ experienced by stars in a spherical system is related to the Newtonian acceleration due to baryons $g_{\mathrm{bar}}(r)$ as

$$g_{\mathrm{dyn}}(r) = \nu\left(\frac{g_{\mathrm{bar}}(r)}{g_†}\right) g_{\mathrm{bar}}(r), \qquad (1)$$

where $\nu(x)$ is known as the MOND interpolating function (IF) defining the RAR in the MOND framework, and $g_†$ is the

acceleration parameter of interest here. We consider

$$\nu(x) = \frac{1}{2} + \sqrt{\frac{1}{4} + \frac{1}{x}}, \qquad (2)$$

which is known as the Simple IF (Famaey & Binney 2005). This particular form seems to be preferred by elliptical galaxies (Chae et al. 2019b); it is similar to the form used by McGaugh et al. (2016) to describe the SPARC galaxies, differing only in a subtle way at relatively high accelerations. Because we intend to test the universality of $g_†$, we do not allow the IF functional form to vary. Our goal of testing the universality of $g_†$ does not depend on this choice of the Simple IF. An alternative choice of the SPARC IF can shift the inferred $g_†$ by an amount smaller than the uncertainty of the global value that we will obtain.

We assume that the projected mass density of stars follows the observed surface brightness distribution with a possible radial variation of $\Upsilon_\star \equiv M_\star/L$ in the inner region $\lesssim 0.8R_e$:

$$\Upsilon_\star(R) = \Upsilon_{\star0} \times \max\{1 + K[A - B(R/R_e)], 1\}, \qquad (3)$$

with $A = 2.33$ and $B = 3$ and K is a parameter representing the strength of a gradient (Chae et al. 2018). As estimated by Bernardi et al. (2018) $K = 1$ corresponds to the strong gradient reported in the literature (van Dokkum et al. 2017), but here we take a mild gradient of $K = 0.21$, i.e., $M_\star/L(R = 0) = 1.5 \times M_\star/L$ ($R \geqslant 0.8R_e$), with a scatter of 0.1 based on Domínguez Sánchez et al. (2019) and Bernardi et al. (2019). However, even if a broad range of $0 < K < 1$ is allowed with a flat prior as in Chae et al. (2019b), it has only a minor impact on our study.

We can link the observed $\sigma_{\mathrm{los}}(R)$ profile with the empirical acceleration $g_{\mathrm{dyn}}(r)$ through the spherical Jeans equation (Binney & Tremaine 2008) and a velocity dispersion anisotropy profile $\beta(r) \equiv 1 - \sigma_t^2(r)/\sigma_r^2(r)$, where $\sigma_r(r)$ and $\sigma_t(r)$ are, respectively, the one-dimensional radial and tangential velocity dispersions. We assume a smoothly varying anisotropy profile of

$$\beta(r) = \beta_0 + (\beta_\infty - \beta_0)\frac{(r/r_a)^2}{1 + (r/r_a)^2}, \qquad (4)$$

where β_0 (β_∞) is the anisotropy at $r = 0$ (∞) and r_a is the radius where the anisotropy is the middle between the two.

Our model has the following free parameters:

$$\vec{\Theta} = \{M_{\star0}(\equiv \Upsilon_{\star0}L), K, \beta_0, \beta_\infty, r_a, g_†\},$$

where L is the luminosity. We impose the following priors: a Gaussian prior with $(\mu, \sigma) = (0.21, 0.1)$ for K, and flat priors $-2 < \beta_0 < 0.7$, $-2 < \beta_\infty < 0.7$, $0.1R_e < r_a < 1R_e$, and $-15 < \log_{10}g_† < -5$ where R_e is the effective radius and $g_†$ is in units of m s^{-2}. In general Bayesian applications, it would be preferable to impose an empirical common prior distribution on $g_†$ estimated from elliptical galaxies themselves. In our study, we carefully selected a clean sample of galaxies with well-determined σ_{los} profiles. This means that $g_†$ may be robustly estimated in each galaxy even when the prior on its value is uninformative. The prior ranges on the other parameters are discussed in Chae et al. (2018, 2019a).

---

[4] In rotationally supported galaxies the observed circular velocity is directly related to the centripetal acceleration via $g = V^2/R$. In dispersion-supported galaxies, the observed line-of-sight velocity dispersion is indirectly related to the radial acceleration via the spherical Jeans equation.

We define a χ^2 function by

$$\chi^2 = \sum_{i=1}^{N_{bin}} \left(\frac{\sigma_{los}^{mod}(R_i) - \sigma_{los}^{obs}(R_i)}{\delta_i} \right)^2, \qquad (5)$$

where $\sigma_{los}^{obs}(R_i)$ and δ_i are the mean and its error in each radial bin from the velocity dispersion map (see Figure 1), and $\sigma_{los}^{mod}(R_i)$ is the MOND model prediction (Chae et al. 2018, 2019b). The likelihood is $\propto e^{-\chi^2/2}$ and the posterior probability density function (PDF) of $g_†$ is derived from Markov Chain Monte Carlo (MCMC) simulations with the public code emcee (Foreman-Mackey et al. 2013). As was discussed in the appendix of Chae et al. (2019b), because of the complexity of the parameter space a narrow distribution of initial walkers around the maximum-likelihood estimate of the parameters can produce unrealistically narrow PDFs. However, if initial walkers are widely distributed within the prior ranges, then the PDFs returned by MCMC widen and become more similar to the results from the simple Monte Carlo simulations discussed by Chae et al. (2019b). Therefore, here we consider only MCMC simulations with widely sampled initial walkers, which are qualitatively similar to the simple Monte Carlo simulations.

3. Results

Figure 2 shows MCMC results for 15 MaNGA E0 galaxies. It shows posterior probability distributions in the g_x/g_{bar} (where $g_x \equiv g_{dyn} - g_{bar}$) versus g_{bar} plane. Note that for the supercritical (i.e., $g_{bar} \gtrsim 10^{-10}$ m s^{-2}) acceleration regime, subtly different cases can be better distinguished in this modified RAR space (Chae et al. 2019b). Similar results for ATLAS^{3D} galaxies can be found in Chae et al. (2019b) and slightly revised results from this work are not shown. Figure 2 indicates that the case with $g_† = 1.2 \times 10^{-10}$ m s^{-2} is included within the 2σ, i.e., 95%, confidence limits (CLs) of every individual galaxy displayed.

The top panel of Figure 3 shows the individual PDFs of $g_†$ for the 19 MaNGA and ATLAS^{3D} E0 SRs sorted in order of ascending $g_†$. As indicated in Figure 2, individual PDFs are quite broad, with 2σ CLs covering ~3 dex. This is, in part, because uninformative priors are used for $g_†$, but reflects the fact that our velocity dispersion profiles probe an acceleration range that is only weakly sensitive to $g_†$.

It is evident from Figure 3 that all PDFs overlap one another well. All PDFs include the global median within 2σ. Also, 12 out of 19 galaxies include the global median within 1σ, i.e., 68%, CL. Thus, our results are statistically consistent with a universal value of $g_†$ among all E0 galaxies. The global median for our E0s $g_† = 1.5_{-0.6}^{+0.9} \times 10^{-10}$ m s^{-2} is in excellent agreement with the canonical value for rotationally supported galaxies $g_† = 1.2 \times 10^{-10}$ m s^{-2}.

As a self-consistency check of our MCMC modeling we have considered other objects for which the spherical model is less well motivated or inadequate. We first consider an extended sample that includes all 16 SRs from the ATLAS^{3D} photometric pure-bulge sample (Chae et al. 2018; i.e., we relax the criterion on the circularity of the light distribution). The bottom panel of Figure 3 shows the individual PDFs for all 31 SRs. Evidently, even non-E0 (i.e., not perfectly round) SRs are consistent with a universal value of $g_†$. This may imply that the spherical model with velocity dispersion anisotropy can
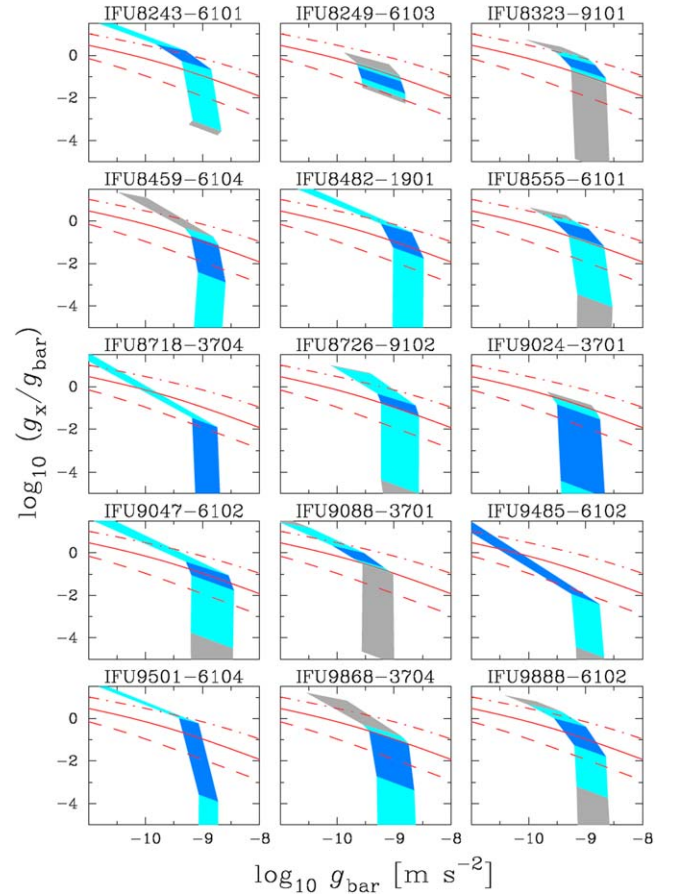

Figure 2. MCMC results for MaNGA E0 SR galaxies. For galaxies with the IFU plate numbers given, the posterior probability distributions from MCMC outputs are shown in a modified RAR space by colored bands: blue 1σ, cyan 2σ, and gray 3σ. Here $g_x \equiv g_{dyn} - g_{bar}$. The width of each band corresponds to a posterior range of $g_†$. The red solid, dashed, and dashed–dotted lines correspond to $g_† = 1.2 \times 10^{-10}$, 1.2×10^{-11}, and 1.2×10^{-9} m s^{-2}.

adequately describe nearly spherical SRs. If we include eight fast-rotator (FR) ATLAS^{3D} galaxies from the sample defined by Chae et al. (2018), then we find two individual results that deviate by more than 3σ from the universal $g_†$ value. Of course, this is not surprising because the spherical model is bound to fail for FRs; rather, it demonstrates self-consistency of our MCMC modeling.

Figure 4 shows 387 data points from the MCMC analysis of the velocity dispersion profiles of the 19 E0s in the top panel of Figure 3 in a format that is similar to the RAR for rotationally supported SPARC galaxies (McGaugh et al. 2016; Lelli et al. 2017). Two tracks from MaNGA IFU 8243-6101 and NGC 4636 appear offset toward larger $g_†$, but these points are actually consistent with the RAR curve within their 2σ uncertainties. These galaxies are not otherwise unusual. Overall, the inset shows that all 387 points are statistically consistent with a universal RAR, confirming the results shown in Figures 2 and 3.

4. Discussion

In light of the recent debate on the presence of a universal acceleration scale involving dark matter phenomena in rotationally supported galaxies (Kroupa et al. 2018; McGaugh et al. 2018; Rodrigues et al. 2018a, 2018b; Chang & Zhou 2019; Marra et al. 2020), we have carried out kinematic analyses of a well-defined sample of E0 SR galaxies. Our
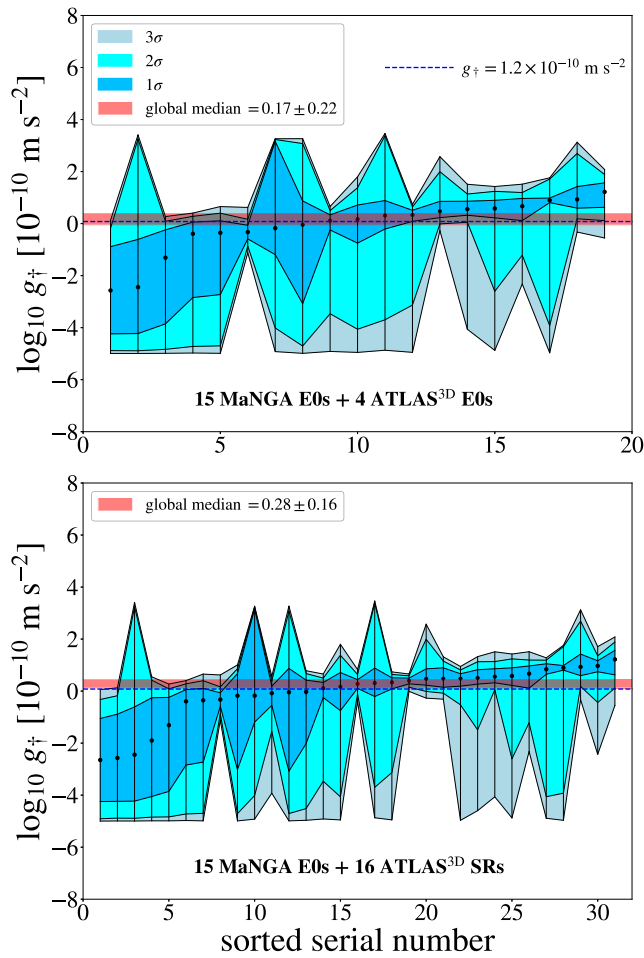
Figure 3. Individually fitted $g_\dagger$ for elliptical galaxies. (Top) Individual PDFs of $g_\dagger$ for E0 SR galaxies selected from SDSS-IV MaNGA and ATLAS[3D]. Individual PDFs are not Gaussian as can be seen by the confidence limits. The global median is defined by the median of the medians from the PDFs and its uncertainty is estimated by bootstrap resampling. All individual PDFs overlap so that all are consistent with the global median within 2σ. (Bottom) This includes 12 ATLAS[3D] non-E0 SRs. The overall statistical properties are similar to the top panel.
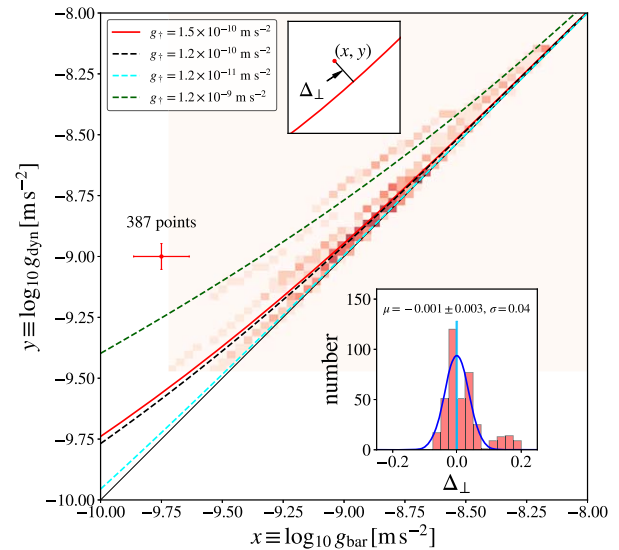

Figure 4. RAR for MaNGA and ATLAS[3D] E0 SR galaxies. Heatmap shows g_{dyn} and g_{bar} for 387 data points from the 19 objects in the top panel of Figure 3. Error bar on the left of the plot shows typical uncertainties from the MCMC results. Curves show Equation (1) for various $g_\dagger$ (as labeled). Histogram in bottom right inset panel shows the distribution of offsets from the red curve; blue curve shows a Gaussian with rms 0.04.

Bayesian inference analysis yields individual posterior PDFs of $g_\dagger$ for 19 E0s that are consistent with a universal value of $g_\dagger = 1.5^{+0.9}_{-0.6} \times 10^{-10}$ m s^{-2}. This value agrees well with that reported by McGaugh et al. (2016) for 153 rotationally supported galaxies from the SPARC database: $g_\dagger = (1.2 \pm 0.2) \times 10^{-10}$ m s^{-2} (including systematic error).

Two crucial aspects of our Bayesian methodology are (1) the selection and use of reliable kinematic data and (2) robust and wide searches of the parameter space within the prior ranges. When these requirements are met, the presence of a common parameter may be tested for statistically. When the estimated error models are uncertain and/or the kinematic model is inappropriate, Bayesian inference is not suitable for statistically testing a common parameter (see also the discussion in Cameron et al. 2020).

To test the universality of $g_\dagger$ in generic early-type galaxy samples, one *must* use accurate nonspherical models. The larger parameter space of such models, and the greater likelihood of parameter degeneracies, will make this challenging. We believe that our results for (very nearly) spherical galaxies, which support the presence of a universal $g_\dagger$ for dark matter phenomena in

galaxies, motivate future efforts to test the universality of $g_\dagger$ in generic galaxy samples, however challenging.

The presence of a universal acceleration scale fits naturally into the MOND paradigm: the empirical $g_\dagger$ becomes Milgrom's critical acceleration a_0. We would have falsified MOND if we had not found a universal value, or if this value had been different from that for rotating galaxies. In this respect, we note that MOND analyses were carried out recently based on MaNGA (Durazo et al. 2018) and ATLAS[3D] (Tortora et al. 2014) galaxies, although our sample is more carefully defined and our analysis, which accounts for $M_\star/L$ radial gradients, is more general. Currently available ΛCDM simulations of galaxy formation and evolution predict intrinsic scatter of $\sim$0.06–0.08 dex in the value of $g_\dagger$ around the empirical mean value (see Stone & Courteau 2019 and references therein, in particular, Dutton et al. 2019). As this is substantially smaller than our current error bars, larger samples are needed to test if this is consistent with the data.

ORCID iDs

Kyu-Hyun Chae ⓘ https://orcid.org/0000-0002-6016-2736
Ravi K. Sheth ⓘ https://orcid.org/0000-0002-2330-0917

References

Aguado, D. S., Ahumada, R., Almeida, A., et al. 2019, ApJS, 240, 23
Bernardi, M., Domínguez Sánchez, H., Brownstein, J. R., Drory, N., & Sheth, R. K. 2019, MNRAS, 489, 5633

Bernardi, M., Sheth, R. K., Dominguez-Sanchez, H., et al. 2018, MNRAS, 477, 2560

Binney, J., & Tremaine, S. 2008, Galactic Dynamics (2nd ed.; Princeton, NJ: Princeton Univ. Press)

Bundy, K., Bershady, M. A., Law, D. R., et al. 2015, ApJ, 798, 7

Cameron, E., Angus, G. W., & Burgess, J. M. 2020, NatAs, 4, 132

Cappellari, M., Emsellem, E., Krajnović, D., et al. 2011, MNRAS, 413, 813

Chae, K.-H., Bernardi, M., & Sheth, R. K. 2018, ApJ, 860, 81

Chae, K.-H., Bernardi, M., & Sheth, R. K. 2019a, ApJ, 874, 41

Chae, K.-H., Bernardi, M., Sheth, R. K., & Gong, I.-T. 2019b, ApJ, 877, 18

Chae, K.-H., Lelli, F., Desmond, H., et al. 2020, ApJ, in press (arXiv:2009.11525)

Chang, Z., & Zhou, Y. 2019, MNRAS, 486, 1658

Djorgovski, S., & Davis, M. 1987, ApJ, 313, 59

Domínguez Sánchez, H., Bernardi, M., Brownstein, J. R., Drory, N., & Sheth, R. K. 2019, MNRAS, 489, 5612

Dressler, A., Lynden-Bell, D., Burstein, D., et al. 1987, ApJ, 313, 42

Durazo, R., Hernandez, X., Cervantes Sodi, B., & Sanchez, S. F. 2018, ApJ, 863, 107

Dutton, A. A., Macciò, A. V., Obreja, A., & Buck, T. 2019, MNRAS, 485, 1886

Faber, S. M., & Jackson, R. E. 1976, ApJ, 204, 668

Famaey, B., & Binney, J. 2005, MNRAS, 363, 603

Fischer, J.-L., Dominguez-Sanchez, H., & Bernardi, M. 2019, MNRAS, 483, 2057

Foreman-Mackey, D., Hogg, D. W., Lang, D., & Goodman, J. 2013, PASP, 125, 306

Kroupa, P., Banik, I., Haghi, H., et al. 2018, NatAs, 2, 925

Lelli, F., McGaugh, S. S., & Schombert, J. M. 2016, AJ, 152, 157

Lelli, F., McGaugh, S. S., Schombert, J. M., & Pawlowski, M. S. 2016, ApJL, 827, L19

Lelli, F., McGaugh, S. S., Schombert, J. M., & Pawlowski, M. S. 2017, ApJ, 836, 152

Li, P., Lelli, F., McGaugh, S., & Schombert, J. 2018, A&A, 615, 70

Marra, V., Rodrigues, D. C., & de Almeida, A. O. F. 2020, MNRAS, 494, 2875

McGaugh, S. S., Lelli, F., & Schombert, J. M. 2016, PhRvL, 117, 201101

McGaugh, S. S., Li, P., Lelli, F., & Schombert, J. M. 2018, NatAs, 2, 924

McGaugh, S. S., & Schombert, J. M. 2014, AJ, 148, 77

McGaugh, S. S., Schombert, J. M., Bothun, G. D., & de Blok, W. J. G. 2000, ApJL, 533, L99

Milgrom, M. 1983, ApJ, 270, 371

Rodrigues, D. C., Marra, V., del Popolo, A., & Davari, Z. 2018a, NatAs, 2, 668

Rodrigues, D. C., Marra, V., del Popolo, A., & Davari, Z. 2018b, NatAs, 2, 927

Schombert, J. M., McGaugh, S. S., & Lelli, F. 2019, MNRAS, 483, 1496

Stone, C., & Courteau, S. 2019, ApJ, 882, 6

Tortora, C., Romanowsky, A. J., Cardone, V., Napolitano, N. R., & Jetzer, Ph. 2014, MNRAS, 438, L46

Tully, R. B., & Fisher, J. R. 1977, A&A, 54, 661

van Dokkum, P., Conroy, C., Villaume, A., Brodie, J., & Romanowsky, A. J. 2017, ApJ, 841, 68